Journal of Materials Chemistry C

ROYAL SOCIETY OF CHEMISTRY

PAPER

View Article Online
View Journal

Cite this: DOI: 10.1039/d0tc00054j

A highly sensitive, stable, scalable pressure sensor based on a facile baking-inspired foaming process for a human–computer interface†

Guk-Jin Jeon, ‡ Hye-In Yeom, ‡ Taiyu Jin, Jingyu Kim, Junghoon Yang and Sang-Hee Ko Park *

Received 5th January 2020,
Accepted 14th February 2020

DOI: 10.1039/d0tc00054j

rsc.li/materials-c

Flexible and wearable pressure sensors, which can detect various pressures generated by the human body and convert them into electrical signals, are of great interest because they have a wide variety of applications for an interface between humans and external devices. Elastomeric dielectric materials for commercial piezocapacitive pressure sensors need to be manufactured quickly and easily *via* cost-effective methods. Herein, we report a piezocapacitive pressure sensor based on a three-dimensional macroporous dielectric layer fabricated by a rapid and facile baking-inspired foaming process. The pressure sensor showed high sensitivities of 0.16 ± 0.03 kPa^{-1} (at <1 kPa) and 0.14 ± 0.02 kPa^{-1} (at 1–10 kPa) and a low detection limit of 9.8 Pa. Furthermore, 10 000 repetitive compressing and releasing cycles confirmed its reliability. We established that the pressure sensor could move virtual fingers by detecting finger gripping pressure in real time. The respiration rate was also detected by the pressure sensor. A large-scale pressure sensor array was constructed to demonstrate a scaled-up fabrication process. The array accurately recognized spatially distributed pressures generated by objects.

Introduction

Wearable physical sensors that can imitate human skin and act as an interface between humans and external devices have received a great deal of attention over the last several decades, as shown by the outstanding developments in various applications such as electronic textiles,[1–4] electronic skins,[5,6] and biological sensors.[7,8] Such physical sensors have mainly been designed and developed to measure and quantify human vital signals; the sensors have the potential for diagnosing diseases without the requirement for a hospital visit, or monitoring of hand motions and touch.[9] The sensors are classified by physical stimulus type, *i.e.*, pressure, strain, temperature, or humidity.[10] Among these various physical stimuli, pressure is readily detectable by humans, so pressure sensors are of particular interest.[11–13] The pressure exerted by the human body can be classified as subtle (<1 kPa), low (1–10 kPa), medium (10–30 kPa), or high (30–100 kPa) pressure.[12] Pressure can typically be detected by piezoresistive,[14,15] piezocapacitive,[16,17] and piezoelectric transduction mechanisms,[18–20] *via* conversion of the pressure stimulus into electrical signals. The piezoresistive and piezocapacitive mechanisms are frequently applied to detect static pressure with high sensitivity and stability; piezoelectric pressure sensors can normally detect changes in pressure instantaneously. Pressure sensors based on these two mechanism are also attractive because of their simple design and the ease of data analysis. Compared with piezoresistive pressure sensors, piezocapacitive pressure sensors have advantages such as a relatively wide pressure-sensing range, high sensitivity in various pressure regimes, and applicability to the gate dielectric layer in a transistor.[11,12,21] Dielectric layers for piezocapacitive sensors have been studied to improve sensitivity in specific pressure regimes.[22–25] The dielectric layer of a pressure sensor requires low modulus, low viscoelasticity, high relative permittivity, and low leakage current to realize a high-performance pressure sensor.[11,26,27] Silicone elastomers, such as polydimethylsiloxane (PDMS) and Ecoflex, have been primarily used for the dielectric layer because they have a moderate dielectric constant, intrinsic flexibility, chemical resistance, thermal stability and biocompatibility.[28–31]

A dielectric layer with a pyramidal microstructure or air gap can be highly sensitive in the subtle- and low-pressure regimes.[32,33] Although this design has been frequently applied to pressure sensors, capacitive pressure sensors with two-dimensional (2D) microstructured elastomeric dielectric layers have a narrow pressure-sensing range due to the limitation in mechanical changes of microstructured parts. Pressure sensors

Department of Materials Science and Engineering, Korea Advanced Institute of Science and Technology (KAIST), 291 Daehak-ro, Yuseong-gu, Daejeon 34141, Republic of Korea. E-mail: shkp@kaist.ac.kr

† Electronic supplementary information (ESI) available. See DOI: 10.1039/d0tc00054j

‡ Guk-Jin Jeon and Hye-In Yeom contributed equally.

with air gaps also have a narrow pressure range, and require a complex patterning process to ensure that the empty space is preserved. Pressure sensors having high sensitivity over a wide pressure-sensing range have typically been fabricated using a hard template or by phase separation; the dielectric layers in these devices have a three-dimensional (3D) and internally porous microstructure.[34–38] The hard template method uses a porous material that is highly soluble in solvent. However, the template dissolves slowly, which is an issue for large-area fabrication. On the other hand, with the phase separation method, the porous structure is formed using materials that have phases differing in hydrophobicity and hydrophilicity; no additional template-removing process is required. Nevertheless, pressure sensors with a dielectric layer based on phase separation show low sensitivity due to their low porosity. Therefore, producing a porous dielectric layer in a simple yet rapid fashion is still needed to realize pressure sensors having high sensitivity and durability. The process of baking bread suggests a possible solution. Many pores are spontaneously formed by CO_2 gas generated during baking. Baked bread can be significantly deformed by application of external mechanical stress due to its 3D porous structure.

Herein, we present a highly stable and sensitive pressure sensor that uses a 3D macroporous dielectric layer fabricated by a facile foaming process inspired by baking. This layer was obtained by simply curing an emulsion of pore precursors and silicone elastomers. The sensitivity of the capacitive pressure sensor was controlled and evaluated by changing the pore size and porosity of the elastomeric dielectric layer. The pressure sensor with the highest porosity exhibited high sensitivities of 0.16 ± 0.03 and 0.14 ± 0.02 kPa^{-1} in the subtle- and low-pressure regimes, respectively, over a wide pressure range of 9.8 Pa to 80 kPa that was limited only by the pressurizing equipment. The capacitive pressure sensor had fast rising/falling response times of 70 ms under 0.4 kPa, and high stability even after 10 000 cycles of compressing and releasing. The pressure sensor could detect human finger gripping pressure and differentiate between the respiration rate before and after exercise. Furthermore, a large-area pressure-sensor array could spatially map the pressure distribution.

Results and discussion

Fabrication of the flexible piezocapacitive pressure sensor first required the preparation of a silver nanowire (AgNW)-embedded PDMS electrode and the PDMS/Ecoflex-based macroporous dielectric layer. Fig. 1 schematically illustrates the fabrication process. The flexible electrode was patterned using a polyethylene terephthalate (PET) mask and covered with PDMS solution to protect the AgNWs (Fig. 1a). Then, $NaHCO_3$ and CH_3COOH solutions were added to the PDMS/Ecoflex solution and mixed to form an emulsion. Curing of the emulsion for less than 1 h in air in an oven yielded a 3D macroporous structure. Since the PDMS/Ecoflex dielectric layer fabricated without $NaHCO_3$ and CH_3COOH solutions has a non-porous structure, the formation

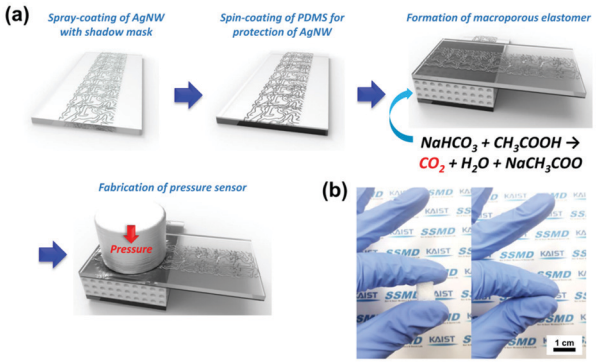

Fig. 1 Preparation of a piezocapacitive pressure sensor with a macroporous PDMS/Ecoflex film. (a) Schematic illustration of the fabrication process based on the reaction of $NaHCO_3$ and CH_3COOH. (b) Photograph of the 3D macroporous PDMS/Ecoflex before and after compression.

of the macroporous structure is attributed to CO_2 generated by the reaction of $NaHCO_3$ and CH_3COOH (Fig. S1, ESI†). This facile and rapid fabrication process for the 3D macroporous dielectric layer is particularly attractive because no additional post-processing or other time-consuming processes are required. The flexible electrodes and 3D macroporous dielectric layer were attached with half-cured PDMS and fully cured. Fig. 1b shows the highly compressive behavior of the macroporous dielectric layer. The amount and density of pores in the dielectric layer could be easily controlled by the curing temperature (T_c) and weight ratio of the $NaHCO_3$ and CH_3COOH solutions mixed into the PDMS/Ecoflex solution (NC concentration). Porosity is an important physical property that is closely related to pressure-sensing performance. First, the effect of T_c on the porosity and pore distribution of the dielectric layer was studied. The emulsion could be formed up to a maximum NC concentration of about 40 wt% in the PDMS/Ecoflex solution; the concentration was set at 38 wt% for the experiments. The dielectric layer had a 3D macroporous structure, provided by CO_2 gas randomly generated during the chemical reaction between $NaHCO_3$ and CH_3COOH. Analysis of the porosity and pore size distribution of a dielectric layer over small (μm-scale) regions can be easily misinterpreted. Therefore, the porosity and pore size distributions were analyzed over large (mm-scale) regions. Fig. 2 shows the porosity and pore size distribution of the elastomeric dielectric layer analyzed by micro-computed tomography (micro-CT). The porosity increased with increasing T_c, from 36% at 80 °C to 69% at 120 °C, which indicated increasing air volume in the solid. When T_c increased from 80 °C to 100 °C, the percent volumes of pores smaller and larger than 404 μm were significantly reduced and increased, respectively (Fig. 2a). When T_c increased from 100 °C to 120 °C, the percent pore volume above 404 μm increased slightly. This indicated that T_c should be about 100 °C for the emulsion to have the appropriate curing condition to form pores larger than 404 μm. The higher T_c increased the vapor pressure of the CO_2 gas generated during the curing process and reduced the reticulation time of the PDMS/Ecoflex, which resulted in the formation of larger pores.[39] Notably, the percent pore volume between 4 and 84 μm diminished with increasing T_c. The $NaHCO_3$ and CH_3COOH

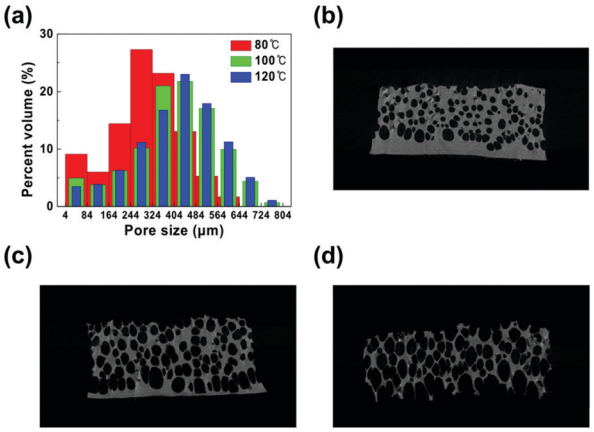

Fig. 2 Micro-CT analysis of the 3D macroporous PDMS/Ecoflex film. (a) Pore size distribution of the film as a function of T_c. Micro-CT cross-section images of the macroporous PDMS/Ecoflex film fabricated under a T_c of (b) 80 °C, (c) 100 °C, and (d) 120 °C.

solutions were present as colloids in the emulsion and reacted during the curing process. This initially led to the formation of CO_2 gas bubbles by nucleation; small pores were the first to be formed during the PDMS/Ecoflex reticulation.[40] Higher T_c likely caused the pores to expand and merge with surrounding pores due to higher CO_2 gas pressure and a coarsening process.[41] The increased pore size with increasing T_c was evident in cross-sectional micro-CT images (Fig. 2b–d). The morphology of the macroporous elastomers was thoroughly characterized by scanning electron microscopy (SEM) (Fig. S2, ESI†). 4–84 μm-sized pores were clearly visible throughout the bulk of the macroporous dielectric layer in high-magnification images. The aforementioned explanation is also in agreement with the results of SEM analysis. The micro-CT and SEM analyses confirmed that the pore size was well-controlled by T_c, which also provided a way to control the porosity.

The influence of T_c on the compressibility of the macroporous elastomers was investigated (Fig. 3a). The elastomer cured at 80 °C showed a significant increase of stress with increasing applied compressive strain. Increasing T_c resulted in a significant reduction in the compressive stress at a given pressure. The elastomer cured at 120 °C maintained a low and linear stress until the compressive strain reached about 50%. The linear moduli were calculated at the compressive strain that corresponded to a compressive stress of 2 kPa.[29] The moduli of elastomers cured at 80 °C, 100 °C, and 120 °C were 26 600 kPa at 7.5% strain, 19.9 kPa at 10% strain and 9.3 kPa at 20% strain, respectively; this indicates that increasing T_c led to a softer elastomer due to higher porosity. When the compressive stress was measured in the forward and reverse directions to evaluate the hysteresis of the elastomers, the hysteresis was unaffected by T_c. This behavior resulted from the limited recovery capability of the PDMS/Ecoflex due to the inherent viscoelasticity of the PDMS/Ecoflex dielectric layer, which caused the mechanical stress of the dielectric layer to be reduced in the reverse sweep.[42,43] Piezocapacitive pressure sensors fabricated with the various macroporous elastomers were characterized to investigate the effect of T_c on their performance. This type of pressure sensor has a capacitor structure with two parallel electrode plates. When an external pressure was applied, the macroporous elastomer became thinner, which increased the capacitance of the sensor. The reversibly compressible behavior of the macroporous elastomer was directly observed by SEM (Fig. S3, ESI†); the elastomers were compressed by narrowing the spacing of the sample-mounting chuck of the instrument. The pore volume gradually reduced with increasing compressive strain. The pores reduced the capacitance of the initial state in the absence of applied pressure due to their low relative permittivity ($\sim$1). The reduction in pore volume increased the net permittivity of the dielectric layer in the pressure sensor, which originated from the reduction of the air volume, resulting in a greater change in capacitance. The lower initial capacitance and increased change in capacitance accelerated the relative capacitance change of the pressure sensor compared with that of a pore-free pressure sensor. Since the morphology of the dielectric layer after removing the compressive strain was the same as the initial state, the macroporous dielectric layer was reversibly compressible, which is very important for pressure sensor stability. The electromechanical response of the pressure sensors was investigated by monitoring the change in capacitance as a function of applied pressure. The macroporous elastomers had a thickness and

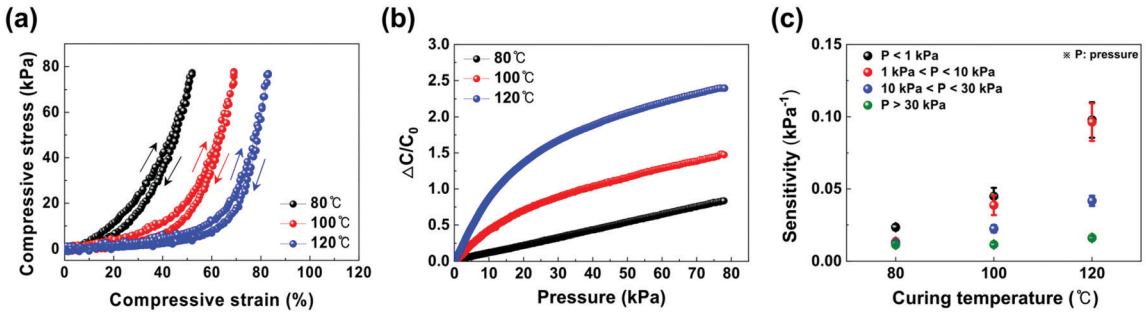

Fig. 3 Characterization of the piezocapacitive pressure sensor based on the 3D macroporous PDMS/Ecoflex elastomer fabricated using an NC concentration of 38 wt% under a T_c of 80 °C, 100 °C, and 120 °C. (a) Compressive stress–strain characteristics of the macroporous PDMS/Ecoflex elastomer as a function of T_c. (b) Relative capacitance change–pressure characteristics of the pressure sensors as a function of T_c. (c) Sensitivities of 10 pressure sensors for different pressure ranges as a function of T_c. The error bars mean the standard deviation.

sensing area of approximately 3 mm and 1 cm^2, respectively. Fig. 3b shows the capacitance change of the pressure sensors with applied pressure as a function of T_c. The capacitance of the pressure sensors increased linearly until reaching a specific pressure, and the slope of the capacitance change gradually decreased with increasing pressure. The capacitance after the specific pressure also linearly increased with a lower slope than the initial state. The response curves of the pressures sensors show a steep slope at low pressures and a gentle slope at high pressures. The capacitance of the pressure sensors with the elastomers cured at higher T_c was very sensitive to the applied pressure. To compare the sensitivity of the pressure sensors in detail, the sensitivity was determined under various pressure regimes, *i.e.*, subtle pressure (1 kPa), low pressure (1–10 kPa,) medium pressure (10–30 kPa), and high pressure (>30 kPa) (Fig. 3c and Fig. S4, ESI†).[12] The sensitivities of the pressure sensors increased under all pressure regimes with increasing T_c. Although the degree of increase in sensitivity with increasing T_c was reduced as the applied pressure transitioned from the subtle- to the high-pressure regime, a higher T_c improved the electromechanical response of the pressure sensor under all pressure regimes. The great improvement in sensitivity under the subtle- and low-pressure regimes is attributed to the significant increase in the number of pores larger than 404 μm (Fig. 2a).

The effect of NC concentration on the performance of the high-sensitivity pressure sensor prepared with a T_c of 120 °C was studied in detail. The NC concentration was varied from 0 wt%, *i.e.*, the pristine PDMS/Ecoflex solution without $NaHCO_3$ and CH_3COOH, to 28, 33, and 38 wt%. Fig. 4 shows the electromechanical response and sensitivity of the pressure sensors as a function of NC concentration. The pressure sensor fabricated with the pristine PDMS/Ecoflex solution displayed the smallest relative capacitance change with applied pressure, due to the poor compressibility of the bulk material (Fig. 4a). In contrast, the addition of $NaHCO_3$ and CH_3COOH significantly increased the relative capacitance change with increasing applied pressure. The sensitivity of the pressure sensors was extracted to allow comparison of their performances under each pressure regime (Fig. 4b and Fig. S5, ESI†). The average sensitivity for the sensors prepared with an NC concentration of 28 wt% was higher than that of the other pressure sensors in the subtle- and low-pressure regimes. The sensitivity decreased with increasing NC concentration; this was especially apparent under the subtle- and low-pressure regimes. On the other hand, the sensitivities of the pressure sensors under the medium- and high-pressure regimes were similar regardless of the NC concentration. To further investigate the origin of the reduced sensitivity, the dielectric layers fabricated with the different NC concentrations were analyzed by micro-CT (Fig. S6a, ESI†). Increasing the NC concentration from 28 to 33 wt% caused the percent volume of pores smaller and larger than 404 μm to significantly increase and decrease, respectively. Increasing the NC concentration to 38 wt% further increased and decreased the percent volume of pores smaller and larger than 404 μm, respectively. The calculated porosity increased by 73%, 72%, and 67% for NC concentrations of 28, 33, and 38 wt%, respectively. The trend in porosity is consistent with that of the pore size distribution. Cross-sectional images confirmed the change in pore size with respect to the NC concentration (Fig. S6b–d, ESI†). A lower NC concentration likely reduced the disturbance of pores during their formation, leading to larger pore sizes. High sensitivity could be achieved easily by increasing T_c and reducing the NC concentration.

The electromechanical response and stability of the pressure sensor fabricated using an NC concentration of 33 wt% and a T_c of 120 °C were determined; these conditions provided optimal uniformity and sensitivity. Fig. 5a displays the response time of the capacitive pressure sensor while applying and relaxing a constant pressure. The magnified images confirm the rising and falling response times (the insets in Fig. 5a). When the pressure sensor was unloaded, the relative capacitance change was well maintained. When the pressure sensor was instantaneously

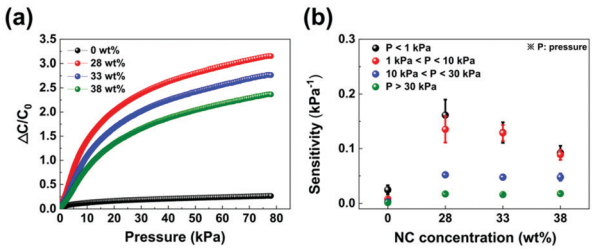

Fig. 4 Characterization of the piezocapacitive pressure sensor based on the macroporous PDMS/Ecoflex film fabricated under a T_c of 120 °C using an NC concentration of 0, 28, 33, and 38 wt%. (a) Relative capacitance change–pressure characteristics of the pressure sensors depending on the NC concentration. (b) Sensitivities of 10 pressure sensors extracted for different pressure ranges as a function of NC concentration. The error bars mean the standard deviation.

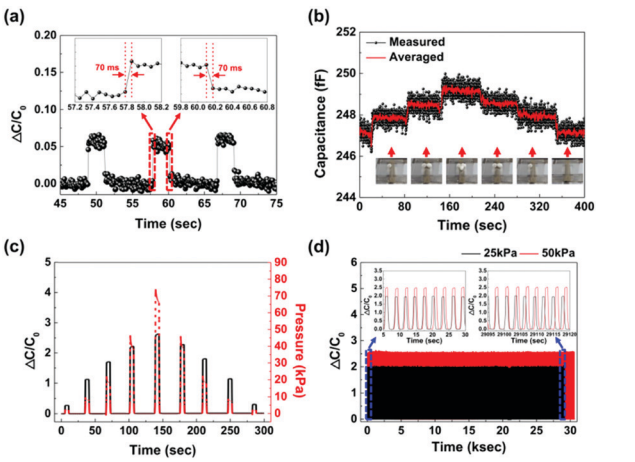

Fig. 5 Pressure-dependent sensing performance of the pressure sensor based on the macroporous PDMS/Ecoflex dielectric layer fabricated under a T_c of 120 °C using an NC concentration of 33 wt%. (a) Pressure response time for repetitive loading and unloading of an applied pressure of 0.4 kPa. The insets show the rising and falling response time. (b) Capacitance response to repetitive loading and unloading of an ultra-light object (10 mg and 9.8 Pa), used to evaluate the limit of detection. (c) Relative capacitance change in response to successive and dynamic pressure changes below 80 kPa. (d) Cyclic response of the pressure sensor over 10 000 cycles under pressures of 25 and 50 kPa.

loaded with 400 Pa at 57.78 s, the relative capacitance change promptly increased, and the elevated capacitance remained nearly constant from 57.85 s onward. The relative capacitance was immediately reduced to that of the initial state after removal of the applied pressure at 60.1 s, and the initial relative capacitance remained constant from 60.17 s. The rising and falling response times were both about 70 ms. The response time was limited by the speed of the pressurizing probe and the sampling rate of the LCR meter; 70 ms response times were the minimum values for our measurement system. Accordingly, the real response time of the capacitive pressure sensors is likely shorter than 70 ms. Higher pressures of 2, 25, and 40 kPa were applied to further investigate the pressure-sensitive response of the pressure sensors (Fig. S7, ESI†). The relative capacitance change closely followed the pressure change regardless of the applied pressure. Additionally, subtle pressure, which could be measured by the capacitive pressure sensor, was demonstrated. Fig. 5b illustrates the limit of detection of the pressure sensor when light-weight (10 mg, 9.8 Pa) objects were placed on top of the sensor. Although the measured capacitance fluctuated from 1 to 1.5 fF due to external noise, there was a distinct difference in capacitance as the number of objects increased or decreased. When the measured capacitance values were averaged using the moving average method, the difference was more noticeable. To simulate a real situation, the dynamic response of the pressure sensors was also examined as various pressures were applied over time. When the applied pressure (<80 kPa) changed in real time, the response output profile matched the pressure input profile, with a stable and completely reversible shape (Fig. 5c). The viscoelastic properties of the elastomer in a pressure sensor can influence its stability due to poor resilience, originating from stress relaxation during constant strain.[44,45] Loading and unloading, with pressures of 25 and 50 kPa, were repeatedly applied to our pressure sensor over 10 000 cycles. Fig. 5d shows that the pressure sensor had excellent durability and stability in the medium- and high-pressure regimes. The results for the initial, middle, and final cycles were almost unchanged, with no remarkable degradation. Table S1 (ESI†) compares the performance of our pressure sensor with those of previously reported porous sensors. Our pressure sensor had similar or better performance as well as the fastest processing time; this is very important for commercialization.

The flexibility and excellent performance of our macroporous pressure sensor enabled its use to detect various signals generated by the human body, such as finger motion and respiration rate. Five pressure sensors were attached to the fingertips to act as the interface between real fingers, and virtual fingers on a computer. The serial connection of the capacitors and the microcontroller unit allowed the acquisition of data from the pressure sensors (Fig. S8, ESI†). As the capacitance of the pressure sensor (C_{sensor}) changed when any object was held with the fingers, the output voltage (V_{out}) also changed because of the serial connection with the reference capacitor (C_{ref}). Thus, C_{sensor} was determined based on V_{out} and the relative capacitance change was internally calculated by the circuit. The angle of the virtual fingers changed with the relative capacitance change value acquired by the circuit. Large

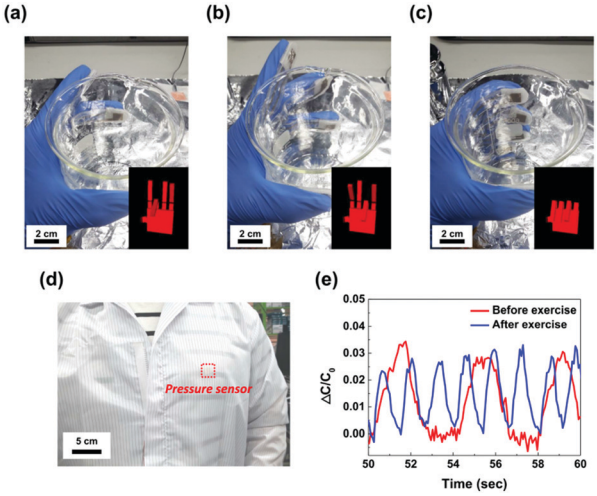

Fig. 6 Real-time sensing performance of the pressure sensor based on the macroporous PDMS/Ecoflex dielectric layer fabricated under a T_c of 120 °C using an NC concentration of 33 wt% for the detection of human motions. (a–c) Photographic images of the virtual fingertip motion corresponding to real fingertip gripping. (d) Photographic image of the pressure sensor attached to the subject's chest for measurement of the respiration rate. (e) Relative capacitance change in response to respiration before and after exercise.

angles of the virtual fingers indicated that the real fingers gripped the object strongly. Fig. 6a–c and Movie S1 (ESI†) demonstrate the motion detection in real time. When the thumb and middle finger held the beaker wall, the virtual fingers were folded at the same position. Likewise, when the thumb and ring finger gripped the beaker wall, the corresponding virtual fingers were folded. All graphic fingers were simultaneously folded when the beaker was gripped with all fingers. It is important to monitor the respiration rate in humans because an abnormal rate can be symptomatic of many diseases.[9] Flexible and wearable sensors are needed to measure the respiration rate because of the large volume and weight of conventional respiratory monitors.[46] Fig. 6d illustrates the placing of the pressure sensor on the chest of a healthy person to detect the respiration rate. The pressure sensor detected the respiration rate *via* chest expansion and contraction. The respiration patterns were measured by the pressure sensor during normal breathing and after exercise (Fig. 6e). Since the normal respiration rate of an adult is about 4 s (including inhalation and exhalation), the measurement result before exercising indicates the normal respiration rate of the subject.

Pressure-sensor arrays (8 × 8) were fabricated using the macroporous dielectric films formed under a T_c of 80 °C and 120 °C, and an NC concentration of 33 wt%, to explore the feasibility of large-area pressure mapping. The area of the macroporous dielectric films was 10 × 10 cm^2 and the relative capacitance change of the central 4 × 4 pixels among 8 × 8 pixels was individually measured under 20 kPa to compare the uniformity of the array between each T_c (Fig. 7a and b). In the central 4 × 4 pixels, the specific positions with the top and bottom electrodes overlapping were pressurized with a force gauge. Fig. 7c and d show that the

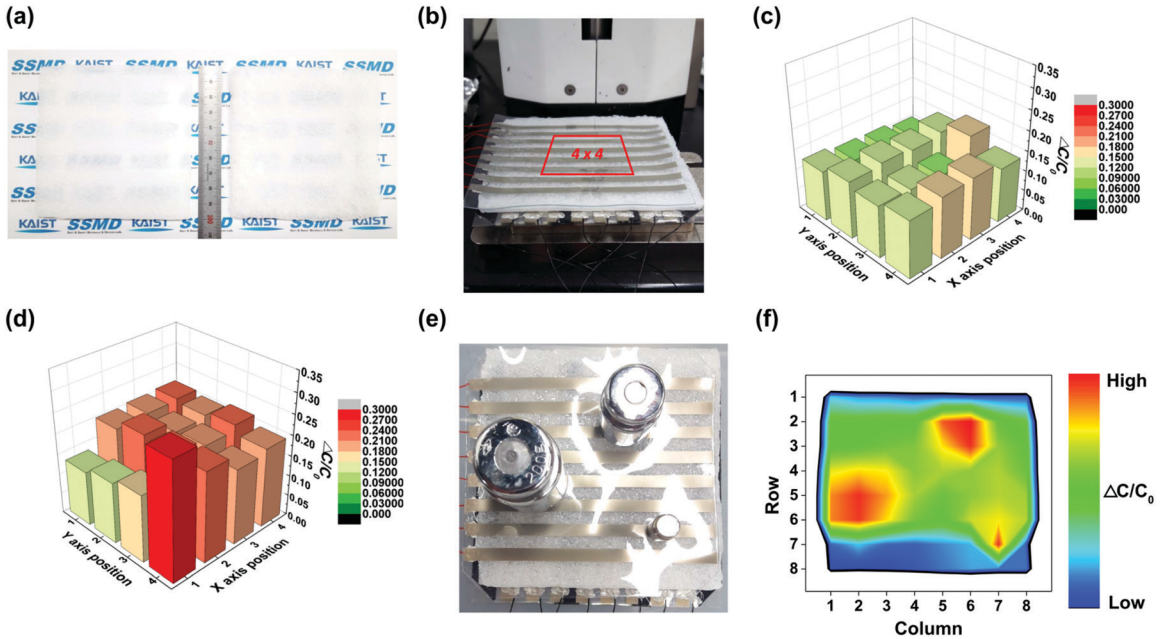

Fig. 7 Large-area sensing performance of the pressure sensor for the measurement of 2D spatial pressure distributions. (a) Photographic image of the macroporous PDMS/Ecoflex dielectric layers fabricated at a T_c of 80 °C (left) and 120 °C (right) using an NC concentration of 33 wt%. (b) An image of the central 4 × 4 pixels used to evaluate array uniformity. Comparison of the pressure sensors based on macroporous PDMS/Ecoflex dielectric layers fabricated under a T_c of (c) 80 °C and (d) 120 °C under 20 kPa. (e) Top view of 10, 100, and 200 g weights placed on an 8 × 8 pressure-sensor array. (f) The 2D pressure distribution corresponding to the applied pressure of the weights acquired by the 8 × 8 pressure-sensor array.

uniformity of the pressure-sensor array fabricated at low T_c was better than that of the array fabricated at high T_c, due to the relatively small and uniform pores as revealed by the micro-CT images. The relative capacitance change of the pressure sensors fabricated under the low and high T_c was 0.135 ± 0.019 and 0.201 ± 0.034, respectively. The coefficient of variation (CV) was calculated by dividing the standard variation into the average in order to quantify the uniformity of the 4 × 4 pixels. The CV of the pressure sensor fabricated at 80 °C was 0.142, while that of the pressure sensor fabricated at 120 °C was 0.172. This indicates that the macroporous dielectric film fabricated at the low T_c was more appropriate for pressure mapping using the sensor array. Three objects with different weights, of 10, 100, and 200 g, were placed on the 8 × 8 sensor array with the dielectric film fabricated under a low T_c to demonstrate the ability to distinguish different pressures (Fig. 7e). Fig. 7f shows the resultant pressure mapping image, drawn according to the relative capacitance change. The position and 2D area in the image are clearly in good agreement with those of the real objects.

Experimental

Preparation of 3D macroporous PDMS/Ecoflex elastomers

The $NaHCO_3$ solution was prepared by stirring and melting $NaHCO_3$ powder at 3 wt% in deionized water (DIW). The CH_3COOH solution was prepared by diluting CH_3COOH solvent at 70 wt% in DIW. PDMS (Sylgard 184; Dow corning) and Ecoflex (0030; Smooth-On) were used as the silicone elastomeric materials for the dielectric layer of the pressure sensor. The PDMS solution was prepared by mixing a base and a curing agent at 10 : 1 w/w. The Ecoflex solution was prepared by mixing a base and a curing agent at 1 : 1 w/w, and the Ecoflex solution was blended with the previously prepared PDMS prepolymer solution at 7 : 3 w/w. The $NaHCO_3$ and CH_3COOH solutions were added dropwise into the PDMS/Ecoflex solution at 28, 33 and 38 wt%, and homogeneously mixed. The weights of the $NaHCO_3$ and CH_3COOH solutions were controlled to maintain the molar ratio at 1 : 1. Tables S2 and S3 (ESI†) show the results for the case when the $NaHCO_3$ and CH_3COOH solutions were incorporated at 33 wt% in the PDMS/Ecoflex solution. Addition of the $NaHCO_3$ and CH_3COOH solutions to the PDMS/Ecoflex solution with stirring formed an emulsion. The emulsion was subsequently cured under a T_c of 80 °C, 100 °C, and 120 °C in an air oven.

Preparation of flexible AgNW electrodes

A PDMS sheet (HT-6240; Rogers Corp.) was used as the substrate to form the flexible AgNW-embedded electrodes. PET was patterned for an electrode mask and placed on the PDMS substrate. The exposed surface of PDMS was treated for 5 min with ultraviolet–ozone (UVO) to render it hydrophilic (Fig. S9, ESI†).[47] An AgNW solution (1 wt%, NANOPYXIS) was spray-coated on the treated PDMS substrate. A PDMS solution was then spin-coated on the AgNW-coated PDMS to protect the AgNW electrode, and cured for 30 min at 100 °C in an air oven.

Characterization

A micro-CT analyzer (SkyScan 1272; Bruker), which uses an X-ray source to nondestructively detect object details larger than 0.45 μm, was used to investigate the true porosity and pore size distributions of the elastomeric dielectric layers. A region larger than the sensing area of the pressure sensor

was analyzed to obtain details of the pressure-sensitive active layer. Morphologies were observed by SEM (Nova230). The mechanical characteristics of the elastomeric dielectric layers were analyzed using an automatic test stand equipped with a force gauge (M5-2; Mark-10). The capacitance change of a pressure sensor was monitored at 400 kHz using an LCR meter (4284A Precision, Hewlett Packard). The data of the force gauge and the LCR meter were simultaneously transmitted to a computer using a customized LabVIEW program.

Conclusions

We developed a highly sensitive and stable piezocapacitive pressure sensor based on a 3D macroporous elastomeric dielectric material fabricated by a rapid and facile baking-inspired foaming process. The macroporous dielectric material could be rapidly formed within 1 h because reticulation of the PDMS/Ecoflex film and the reaction of $NaHCO_3$ and CH_3COOH occurred simultaneously during the curing process. The porosity of the elastomeric dielectric material was readily controlled by T_c and the NC concentration; the dielectric material displayed excellent compressibility and recovery. The best pressure sensor containing a macroporous dielectric layer exhibited high sensitivities of 0.16 ± 0.03 kPa^{-1} (at <1 kPa) and 0.14 ± 0.02 kPa^{-1} (at 1–10 kPa) over pressures ranging from 9.8 Pa to 80 kPa. The sensor responded immediately to applied pressures above 400 Pa, and within 70 ms for applied pressures under 400 Pa. High durability of the sensor was confirmed for 10 000 repetitive loading and unloading cycles. The sensor detected how strongly a person was gripping an object by sensing finger pressure. Additionally, the user's respiration rate was measured to determine whether the user was breathing normally. Finally, large-area pressure-sensor arrays were fabricated to sense spatially distributed pressure. The sensor array distinguished the position and area of the pressure produced by objects differing in weight and size. Our results demonstrate that the elastomeric dielectric material provided high sensitivity and stability to a piezocapacitive pressure sensor, and that the sensor could be rapidly and easily fabricated using a baking-inspired foaming process. A pressure sensor with a 3D macroporous dielectric layer would confer many benefits for applications such as electronic skins and wearable pressure-sensitive devices.

Conflicts of interest

There are no conflicts to declare.

Acknowledgements

This research was supported by the Wearable Platform Materials Technology Center (WMC) funded by the National Research Foundation of Korea (NRF) Grant by the Korean Government (MSIT) (No. 2016R1A5A1009926) and the Nano-Material Technology Development Program through the NRF funded by the Ministry of Science, ICT and Future Planning (2016M3A7B4905609).

References

1 J. Lee, H. Kwon, J. Seo, S. Shin, J. H. Koo, C. Pang, S. Son, J. H. Kim, Y. H. Jang, D. E. Kim and T. Lee, *Adv. Mater.*, 2015, **27**, 2433–2439.
2 M. Liu, X. Pu, C. Jiang, T. Liu, X. Huang, L. Chen, C. Du, J. Sun, W. Hu and Z. L. Wang, *Adv. Mater.*, 2017, **29**, 1703700.
3 Z. Zhou, Y. Li, J. Cheng, S. Chen, R. Hu, X. Yan, X. Liao, C. Xu, J. Yu and L. Li, *J. Mater. Chem. C*, 2018, **6**, 13120–13127.
4 R. Wu, L. Ma, C. Hou, Z. Meng, W. Guo, W. Yu, R. Yu, F. Hu and X. Y. Liu, *Small*, 2019, **15**, 1901558.
5 S. H. Jeong, S. Zhang, K. Hjort, J. Hilborn and Z. Wu, *Adv. Mater.*, 2016, **28**, 5830–5836.
6 Z. Zhu, R. Li and T. Pan, *Adv. Mater.*, 2018, **30**, 1705122.
7 Y. Kim, A. Chortos, W. Xu, Y. Liu, J. Y. Oh, D. Son, J. Kang, A. M. Foudeh, C. Zhu, Y. Lee, S. Niu, J. Liu, R. Pfattner, Z. Bao and T.-W. Lee, *Science*, 2018, **360**, 998–1003.
8 C. Wan, G. Chen, Y. Fu, M. Wang, N. Matsuhisa, S. Pan, L. Pan, H. Yang, Q. Wan, L. Zhu and X. Chen, *Adv. Mater.*, 2018, **30**, 1801291.
9 Y. Khan, A. E. Ostfeld, C. M. Lochner, A. Pierre and A. C. Arias, *Adv. Mater.*, 2016, **28**, 4373–4395.
10 T. Q. Trung and N.-E. Lee, *Adv. Mater.*, 2016, **28**, 4338–4372.
11 M. L. Hammock, A. Chortos, B. C.-K. Tee, J. B.-H. Tok and Z. Bao, *Adv. Mater.*, 2013, **25**, 5997–6038.
12 Y. Zang, F. Zhang, C.-A. Di and D. Zhu, *Mater. Horiz.*, 2015, **2**, 140–156.
13 X. Wang, L. Dong, H. Zhang, R. Yu, C. Pan and Z. L. Wang, *Adv. Sci.*, 2015, **2**, 1500169.
14 L. Pan, A. Chortos, G. Yu, Y. Wang, S. Isaacson, R. Allen, Y. Shi, R. Dauskardt and Z. Bao, *Nat. Commun.*, 2014, **5**, 3002.
15 W. Liu, N. Liu, Y. Yue, J. Rao, C. Luo, H. Zhang, C. Yang, J. Su, Z. Liu and Y. Gao, *J. Mater. Chem. C*, 2018, **6**, 1451–1458.
16 S. Park, H. Kim, M. Vosgueritchian, S. Cheon, H. Kim, J. H. Koo, T. R. Kim, S. Lee, G. Schwartz, H. Chang and Z. Bao, *Adv. Mater.*, 2014, **26**, 7324–7332.
17 K. Lee, J. Lee, G. Kim, Y. Kim, S. Kang, S. Cho, S. Kim, J.-K. Kim, W. Lee, D.-E. Kim, S. Kang, D. Kim, T. Lee and W. Shim, *Small*, 2017, **13**, 1700368.
18 S. Vishniakou, B. W. Lewis, X. Niu, A. Kargar, K. Sun, M. Kalajian, N. Park, M. Yang, Y. Jing, P. Brochu, Z. Sun, C. Li, T. Nguyen, Q. Pei and D. Wang, *Sci. Rep.*, 2013, **3**, 2521.
19 C. Dagdeviren, Y. Su, P. Joe, R. Yona, Y. Liu, Y.-S. Kim, Y. Huang, A. R. Damadoran, J. Xia, L. W. Martin, Y. Huang and J. A. Rogers, *Nat. Commun.*, 2014, **5**, 4496.
20 R. Bao, C. Wang, L. Dong, R. Yu, K. Zhao, Z. L. Wang and C. Pan, *Adv. Funct. Mater.*, 2015, **25**, 2884–2891.
21 A. Chortos, J. Liu and Z. Bao, *Nat. Mater.*, 2016, **15**, 937.
22 S. Baek, H. Jang, S. Y. Kim, H. Jeong, S. Han, Y. Jang, D. H. Kim and H. S. Lee, *RSC Adv.*, 2017, **7**, 39420–39426.
23 H. Kim, G. Kim, T. Kim, S. Lee, D. Kang, M.-S. Hwang, Y. Chae, S. Kang, H. Lee, H.-G. Park and W. Shim, *Small*, 2018, **14**, 1703432.
24 J. Kim, E.-F. Chou, J. Le, S. Wong, M. Chu and M. Khine, *Adv. Healthcare Mater.*, 2019, **8**, 1900109.

25 M. L. Jin, S. Park, Y. Lee, J. H. Lee, J. Chung, J. S. Kim, J.-S. Kim, S. Y. Kim, E. Jee, D. W. Kim, J. W. Chung, S. G. Lee, D. Choi, H.-T. Jung and D. H. Kim, *Adv. Mater.*, 2017, **29**, 1605973.
26 S. C. B. Mannsfeld, B. C. K. Tee, R. M. Stoltenberg, C. V. H. H. Chen, S. Barman, B. V. O. Muir, A. N. Sokolov, C. Reese and Z. Bao, *Nat. Mater.*, 2010, **9**, 859–864.
27 W. Cheng, L. Yu, D. Kong, Z. Yu, H. Wang, Z. Ma, Y. Wang, J. Wang, L. Pan and Y. Shi, *IEEE Electron Device Lett.*, 2018, **39**, 1069–1072.
28 M. C. Bélanger and Y. Marois, *J. Biomed. Mater. Res.*, 2001, **58**, 467–477.
29 A. P. Gerratt, H. O. Michaud and S. P. Lacour, *Adv. Funct. Mater.*, 2015, **25**, 2287–2295.
30 J. Chen, J. Zheng, Q. Gao, J. Zhang, J. Zhang, O. M. Omisore, L. Wang and H. Li, *Appl. Sci.*, 2018, **8**, 345.
31 Z. Lou, L. Wang and G. Shen, *Adv. Mater. Technol.*, 2018, **3**, 1800444.
32 B. C.-K. Tee, A. Chortos, R. R. Dunn, G. Schwartz, E. Eason and Z. Bao, *Adv. Funct. Mater.*, 2014, **24**, 5427–5434.
33 Y. Zang, F. Zhang, D. Huang, X. Gao, C.-A. Di and D. Zhu, *Nat. Commun.*, 2015, **6**, 6269.
34 S. Jung, J. H. Kim, J. Kim, S. Choi, J. Lee, I. Park, T. Hyeon and D.-H. Kim, *Adv. Mater.*, 2014, **26**, 4825–4830.
35 B.-Y. Lee, J. Kim, H. Kim, C. Kim and S.-D. Lee, *Sens. Actuators, A*, 2016, **240**, 103–109.
36 D. Kwon, T.-I. Lee, J. Shim, S. Ryu, M. S. Kim, S. Kim, T.-S. Kim and I. Park, *ACS Appl. Mater. Interfaces*, 2016, **8**, 16922–16931.
37 S. Kang, J. Lee, S. Lee, S. Kim, J.-K. Kim, H. Algadi, S. Al-Sayari, D.-E. Kim, D. Kim and T. Lee, *Adv. Electron. Mater.*, 2016, **2**, 1600356.
38 J. I. Yoon, K. S. Choi and S. P. Chang, *Microelectron. Eng.*, 2017, **179**, 60–66.
39 R. Riesco, L. Boyer, S. Blosse, P. M. Lefebvre, P. Assemat, T. Leichle, A. Accardo and L. Malaquin, *ACS Appl. Mater. Interfaces*, 2019, **11**, 28631–28640.
40 D. L. Tomasko, A. Burley, L. Feng, S.-K. Yeh, K. Miyazono, S. Nirmal-Kumar, I. Kusaka and K. Koelling, *J. Supercrit. Fluids*, 2009, **47**, 493–499.
41 S. Costeux, *J. Appl. Polym. Sci.*, 2014, **131**, 41293.
42 Y. Hsu, K. Lucas, D. Davis, B. Elolampi, R. Ghaffari, C. Rafferty and K. Dowling, *IEEE Trans. Electron Devices*, 2013, **60**, 2338–2345.
43 A. Rinaldi, A. Tamburrano, M. Fortunato and M. S. Sarto, *Sensors*, 2016, **16**, 2148.
44 J. S. Bergström and M. C. Boyce, *J. Mech. Phys. Solids*, 1998, **46**, 931–954.
45 D. Y. Choi, M. H. Kim, Y. S. Oh, S.-H. Jung, J. H. Jung, H. J. Sung, H. W. Lee and H. M. Lee, *ACS Appl. Mater. Interfaces*, 2017, **9**, 1770–1780.
46 M. Chu, T. Nguyen, V. Pandey, Y. Zhou, H. N. Pham, R. Bar-Yoseph, S. Radom-Aizik, R. Jain, D. M. Cooper and M. Khine, *npj Digit. Med.*, 2019, **2**, 8.
47 A. E. Özçam, K. Efimenko and J. Genzer, *Polymer*, 2014, **55**, 3107–3119.

